Published in Applied Physics Letters 56, issue 24, 2448-2450, 1990
which should be used for any reference to this work

Deposition-induced defect profiles in amorphous hydrogenated silicon

N. Hata[a] and S. Wagner
Department of Electrical Engineering, Princeton University, Princeton, New Jersey 08544

P. Roca i Cabarrocas
Laboratoire de Physique des Interfaces et des Couches Minces, Ecole Polytechnique, F-91128 Palaiseau, Cedex, France

M. Favre
Institute of Microtechnology, University of Neuchâtel, CH-2000-Neuchâtel, Switzerland

The thickness dependence of the subgap optical absorption in plasma-deposited hydrogenated amorphous silicon is carefully studied by photothermal deflection spectroscopy. The deep-level defect concentration decays from the top surface into the bulk where it approaches the thermal equilibrium defect density. This defect profile is interpreted in terms of the annealing, during growth, of growth-induced surface defects. It is also shown that this defect profile is compatible with the known growth-temperature dependence of the defect density in amorphous silicon.

The depth distribution of the deep-level defects in amorphous hydrogenated silicon (*a*-Si:H) has been a subject of discussion since the beginning of quantitative measurements of defect density. The contribution of a high density of surface defects to the electron spin resonance (ESR) determined number of unpaired spins as well as to the photothermal deflection (PDS) determined subgap optical absorption were recognized early.[1,2] A controversy followed about a layer at the substrate interface that is particularly susceptible to light-induced defects.[3,4] A detailed evaluation of the thickness dependence of the defect density determined by PDS as a function of film thickness pointed to a thin, defective region at the substrate interface and to a wide region at the top surface.[5] Another observation which suggested a defect profile is that of very low defect densities in very thick films.[6] Growth experiments in SiF_4-H_2 showed that the density of surface states can be varied over two orders of magnitude, and that the surface states maintained during growth can affect the bulk defect density and the width of valence-band tail.[7]

In this letter, we first inspect the defect density of a number of *a*-Si:H films spanning a thickness range of nearly four orders of magnitude. Then we set up a quantitative model for surface-derived defects. In the model we assume that during film growth a steady-state density of surface states is maintained, and that these states decay into the bulk of the film. We set the steady-state density to the value for the density of surface states at thermal equilibrium, 4×10^{17} cm^{-3}.[8] This value is higher than the equilibrium density in the bulk,[9] because the surface defect lies only $\sim$0.57 eV above the valence-band edge,[8] in contrast to the bulk defect at $\sim$0.85 eV. When the surface becomes covered with subsequent layers, the defect energy shifts from 0.57 to 0.85 eV, and the defect density begins to relax to the lower bulk equilibrium value. The resulting defect profile is governed by the density of surface states, the rate of decay, and the rate of film growth. We assume that the decay process is monomolecular and determined by the same kinetics as the annealing of bulk defect states.

[a] On leave from Electrotechnical Laboratory, Ibaraki 305, Japan.

We begin a study of the defect density in a series of samples whose deposition conditions are listed in Table I.[10,11] The densities were determined by PDS which is sensitive to both bulk and surface states.[12,13] The number of defects per unit film area N_s (cm^{-2}) is plotted against the thickness of the films on a log-log scale in Fig. 1. Each data point corresponds to one film. The squares and circles in the figure represent the defect densities of films deposited in the very high frequency (VHF) system at T_d = 190–230 °C, the triangles and crosses in the isothermal rf machine at T_d = 200 °C and T_d = 100 °C, respectively. Three regions are evident even with the wide scatter among the points. We discuss these regions using the series of samples shown as filled squares. In the first region, up to a few tenths of μm film thickness, the total defect density increases as the films are made thicker, a consequence of a density that decays from the surface into the film. The samples in a second region, of intermediate thickness, contain the entire profile of surface-related states. No more of these are added as the thickness is raised, so that the total defect density remains constant. In the third region of very thick films, the total defect density in the bulk becomes comparable to that of the surface-related defects, so that the former begins to make a noticeable contribution.

The increase of the defect density in the lowest thickness range can be interpreted either as top surface or as substrate interface defects decaying over about 0.1 μm. Winer and Ley

TABLE I. Deposition conditions for the *a*-Si:H samples.

Reactor	rf hot wall[a]	VHF glow discharge[b]
Power source frequency	13.56 MHz	38,70,130 MHz
Discharge power density	3 mW/cm^2	50–100 mW/cm^3
SiH_4 flow rate	12 sccm	20 sccm
Deposition pressure	50 mTorr	150–300 mTorr
Growth temperature	100 and 200 °C	190–230 °C
Growth rate	0.5–1 A/s	14–23 A/s
Symbol in Fig. 1	triangles, crosses	squares, circles

[a] Reference 10.
[b] Reference 11.

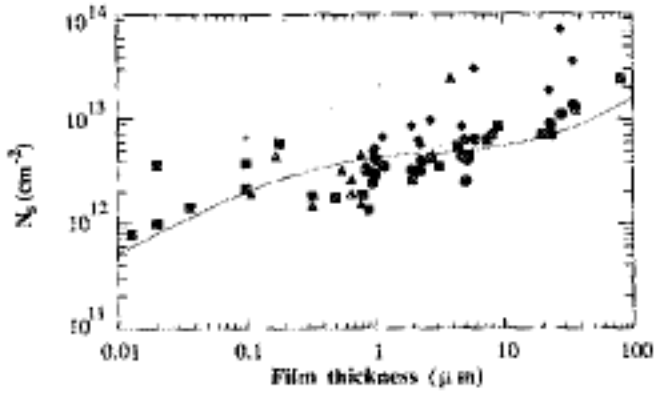

FIG. 1. Area density of deep-level defects determined by PDS measurements plotted against thickness. VHF system at T_s = 190–230 °C (squares and circles); isothermal rf system at T_s = 200 and 100 °C (triangles and cross). The solid line is calculated from Eqs. (7) and (8) for T_d = 230 °C.

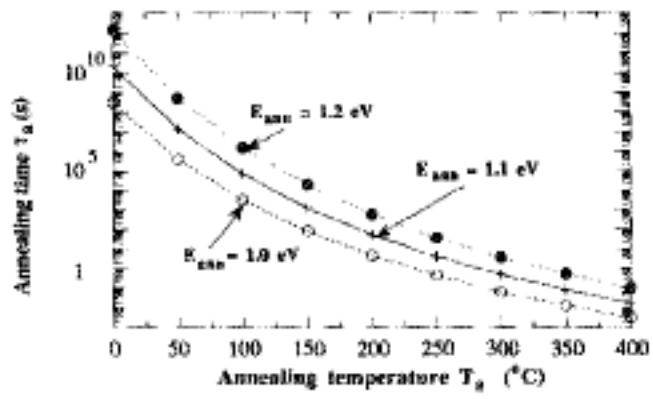

FIG. 2. Annealing time τ_a defined by Eq. (3) plotted against annealing temperature T_a with annealing energy E_{ann} as a parameter.

measured a surface-state density of 8×10^{17} cm^{-3} by total yield photoemission.[14] By PDS experiments, Frye *et al.* measured a high top surface defect density.[15] Maruyama *et al.* demonstrated that the dominant surface-related states are located at the top of the film because their density is reduced by *in situ* annealing after growth.[7] Although Curtins *et al.* detected top and substrate surface defects, the top surface defects dominated.[5] All of these experiments suggest that the increase of defect density in the lowest thickness range results from a profile of top surface defects.

Let us assume a steady-state surface defect density N_s during film growth, and the annealing energy distribution $f_{ann}(E_{ann})$ used previously for light-induced defects,[16] i.e.,

$$f_{ann}(E_{ann}) = (2\pi W^2)^{-1/2}\exp\{-[(E_{ann}-E_0)/W]^2/2\}, \quad (1)$$

where E_{ann}, E_0, and W are the annealing energy, the center of the annealing energy distribution, and the width of the distribution, respectively. Then the rate of annealing of defect states is expressed as

$$\frac{dN(E_{ann})}{dt} = -N(E_{ann})\nu_{ann}\exp\left(\frac{-E_{ann}}{kT}\right), \quad (2)$$

where $N(E_{ann})$, ν_{ann}, k, and T express the density of defects with annealing energy E_{ann}, the attempt frequency for annealing, the Boltzmann constant, and the annealing temperature, respectively.

After defining the annealing time $\tau_{ann}(E_{ann})$ as

$$\tau_{ann}(E_{ann}) = 1/\nu_{ann}\exp(-E_{ann}/kT), \quad (3)$$

we can rewrite Eq. (2) in the simple form of

$$\frac{dN(E_{ann})}{dt} = \frac{-N(E_{ann})}{\tau_{ann}(E_{ann})}. \quad (4)$$

Figure 2 shows the calculated temperature dependence of the annealing time for annealing energies of 1.0, 1.1, and 1.2 eV. Below 200 °C, the annealing time differs by more than two orders of magnitude between the annealing energies of 1.0 and 1.2 eV.

In an amorphous silicon film deposited at the rate of r_d, the *a*-Si:H at the depth L from the top surface of the deposited film underwent annealing for the time L/r_d at the deposition temperature T_d. Therefore, the defect density $N(E_{ann},L)$ as a function of E_{ann} and L is obtained from Eq. (4) as

$$N(E_{ann},L) = N_d f(E_{ann})\exp[-L/r_d\tau_{ann}(E_{ann})]. \quad (5)$$

Defining the deposition time t_d as

$$t_d = L_0/r_d, \quad (6)$$

where L_0 is the total film thickness, and integrating Eq. (5) over the whole range of E_{ann} and time, we obtain the average defect density per area N_s of a film as

$$N_s(T_d,t_d) = \int_0^{t_d}\int_{-\infty}^{+\infty} r_d N(E_{ann},r_d t)\,dE_{ann}\,dt$$
$$= \int_0^{+\infty} r_d N_d f(E_{ann})\tau_{ann}(E_{ann})\times\{1-\exp[-t_d/\tau_{ann}(E_{ann})]\}dE_{ann}, \quad (7)$$

which can be calculated numerically.

In the range of large thickness (> 10 μm), the defect density of amorphous silicon is dominated by the equilibrium density of defect states,[9] which is expressed by the equation

$$N_s(T_d) = [4N_{Si}\exp(-2E_{D^+/D_0}/kT)]^{[kT/(2E_u+kT)]}\times N_{cm}E_u^{[2E_u/(kT+2E_u)]}, \quad (8)$$

where N_{Si}, E_{D^+/D_0}, E_u, and N_{cm} are the density of silicon atoms, the formation energy of the dangling bond state, the Urbach energy, and the density of states at the valence-band mobility edge, respectively.

For numerical calculation, the values of N_{s0}, E_0, W, ν_{ann}, N_{Si}, E_{D^+/D_0}, E_u, and N_{cm} were taken as 4×10^{17} cm^{-3}, 1.05 eV, 0.1 eV, 10^{10} s^{-1}, 4×10^{22} cm^{-3}, 0.85 eV, 50 meV, and 4×10^{21} cm^{-3} eV^{-1}, respectively.[9,16]

The calculated curve for T_d = 230 °C is shown as the solid line in Fig. 1. the calculated curve fits the experimental data points well, which means that the defect density is dominated by the annealing of deposition-induced surface defects in thin films, and by the equilibrium defect density for thick films.

The model also explains the high average defect density in films grown at low, suboptimal, deposition temperature. The slow annealing of growth-induced states at low temperature results in a high defect density throughout the film. Thus, at low temperature (Fig. 1), the density of surface-induced states dominates. The curve in Fig. 3 calculated

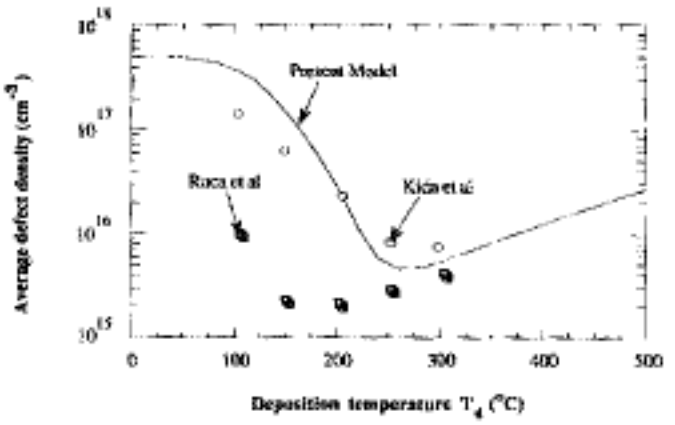

FIG. 3. Calculated average defect density (solid line) as a function of deposition temperature T_d. Circles and squares are experimental data reported in Refs. 17 and 18.

from Eqs. (7) and (8), reflects these two counteracting trends. Experimental results[17,18] on the defect density as a function of growth temperature are also shown. While the temperature dependence agrees, the difference in absolute values between experiments and theory suggests that we need more precise measurements of deposition temperature.

Conventionally, the high defect density in films grown at low substrate temperature has been explained by thermal equilibrium between a high density of valence-band tail states and a correspondingly high N_s.[9,19] Indeed, E_u in low substrate-temperature films is high and so, apparently, is the density of valence-band tail states. However, inspection of the optical absorption spectra (for example, Ref. 17) reveals that a large contribution by N_s raises E_u far above the characteristic energy of the valence-band tail states.[5] In our opinion, the tail state density is much smaller than the measured E_u, and corresponds to values of N_s that are lower than the observed ones.

The physical origin of the high defect density at low temperature is the slow rate of annealing of the deposition-induced defects during film growth. The slow rate is shown in Fig. 2. At the annealing temperature of 200 °C, the annealing time is only a few seconds for an annealing energy of 1.0 eV, and it is less than 1000 s for 1.2 eV. In that sense, most of the deposition-induced defects are annealed out during deposition, and only a few hundred angstroms of a defect-rich surface layer remain. On the other hand, at the annealing temperature of 100 °C, the annealing time is longer than the deposition time (10^4 s) for an annealing energy of 1.1 eV or more, and it is a few thousandths of a second even for 1.0 eV, which means that most of the deposition-induced defects remain throughout the film thickness.

The present model of deposition-induced defect annealing during deposition explains the defect density profile and the average defect density in *a*-Si:H grown at low deposition temperature. The profile cannot be interpreted with the thermal equilibration model. The combination of the decaying surface-state model and the thermal equilibrium model now is a powerful tool for modeling defect densities in amorphous silicon.

We would like to thank N. Wyrsch for his help in procuring one group of samples. We gratefully acknowledge the support of the work at Princeton University by the Electric Power Research Institute.

[1]J. C. Knights, D. K. Biegelsen, and I. Solomon, Solid-State Commun. **22**, 133 (1977).
[2]W. B. Jackson, D. K. Biegelsen, R. J. Nemanich, and J. C. Knights, Appl. Phys. Lett. **42**, 105 (1983).
[3]M. Stutzmann, W. B. Jackson, and C. C. Tsai, Phys. Rev. B **32**, 23 (1985).
[4]S. Guha, W. den Boer, S. C. Agarwall, and M. Hack, Phys. Rev. B **33**, 2512 (1986).
[5]H. Curtins and M. Favre, in *Advances in Disordered Semiconductors*, "Amorphous Silicon and Related Materials", edited by H. Fritzsche (World Scientific, Singapore, 1989), Vol. A, p. 329.
[6]R. A. Street and K. Winer, in *Materials Research Society Proceedings Vol. 149*, "Amorphous Silicon Technology— 1989" edited by A. Madan, M. J. Thompson, P. C. Taylor, Y. Hamakawa, and P. G. LeComber (MRS, Pittsburgh, PA, 1989), Vol. 149, p. 131.
[7]A. Maruyama, J. Z. Liu, V. Chu, D. S. Shen, and S. Wagner, in *Materials Research Society Proceedings*, "Amorphous Silicon Technology-1989", edited by A. Madan, M. J. Thompson, P. C. Taylor, Y. Hamakawa, and P. G. LeComber (MRS, Pittsburgh, PA, 1989), Vol. 149, p. 705.
[8]S. Aljishi, S. Jin, L. Ley, and S. Wagner (unpublished).
[9]Z. E. Smith and S. Wagner, Phys. Rev. Lett. **59**, 688 (1987).
[10]P. Roca i Cabarrocas, These de l'Universite Paris VII, Paris (1988).
[11]H. Curtins, N. Wyrsch, M. Favre, and A. V. Shah, Plasma Chem. Plasma Process. **7**, 2267 (1987).
[12]W. B. Jackson and N. M. Amer, Phys. Rev. B **25**, 5559 (1982).
[13]Z. E. Smith, V. Chu, K. Shepherd, S. Aljishi, D. Slobodin, J. Kolodzey, S. Wagner, and T. L. Chu, Appl. Phys. Lett. **50**, 1521 (1987).
[14]K. Winer and L. Ley, in *Advances in Disordered Semiconductors-Vol. 1*, Amorphous Silicon and Related Materials, Vol. A, edited by H. Fritzsche (World Scientific, Singapore, 1989), p. 365.
[15]R. C. Frye, J. J. Kumler, and C. C. Wong, Appl. Phys. Lett. **50**, 101 (1987).
[16]Z. E. Smith and S. Wagner, Phys. Rev. B **32**, 5510 (1985).
[17]H. Kida, H. Yamagishi, T. Kamada, H. Okamoto, and Y. Hamakawa, in *First International Photovoltaic Science and Engineering Conference*, edited by M. Konagai (Secretariat of International PVSEC-1, Tokyo, 1984), p. 417.
[18]P. Roca i Cabarrocas, J. Z. Liu, H. R. Park, A. Maruyama, and S. Wagner, J. Non-Cryst. Solids **114**, 190 (1989).
[19]M. Stutzmann, Philos. Mag B **60**, 531 (1989).